Geophysical Research Letters

RESEARCH LETTER
10.1029/2018GL080365

Key Points:
- Three-dimensional structure of the eclipse-induced ionospheric electron density depletion was revealed
- The 2017 August solar eclipse halved the electron density in the *F* region with a peak height at 200 km
- Ionospheric TEC decrease and enhancement up to 1.4–1.9 TECU and 0.7–1.0 TECU, respectively, were observed in the geomagnetic conjugate region

Supporting Information:
- Supporting Information S1

Correspondence to:
L. He,
heliming@mail.neu.edu.cn

Citation:
He, L., Heki, K., & Wu, L. (2018). Three-dimensional and trans-hemispheric changes in ionospheric electron density caused by the great solar eclipse in North America on 21 August 2017. *Geophysical Research Letters*, *45*, 10,933–10,940. https://doi.org/10.1029/2018GL080365

Received 5 SEP 2018
Accepted 10 OCT 2018
Accepted article online 15 OCT 2018
Published online 29 OCT 2018

Three-Dimensional and Trans-Hemispheric Changes in Ionospheric Electron Density Caused by the Great Solar Eclipse in North America on 21 August 2017

Liming He[1], Kosuke Heki[2], and Lixin Wu[3]

[1]Department of Geodesy and Geomatics, School of Resources and Civil Engineering, Northeastern University, Shenyang, China, [2]Department of Earth and Planetary Sciences, Hokkaido University, Sapporo, Japan, [3]School of Geosciences and Info-Physics, Central South University, Changsha, China

Abstract We report the three-dimensional (3-D) structure of the electron depletion caused by the great solar eclipse on 21 August 2017 derived from dense Global Navigation Satellite Systems (GNSS) total electron content observations. A linear least squares inversion was performed with a continuity constraint to stabilize the solution. The reconstructed 3-D ionospheric electron density depletion showed a peak height at ~200 km. The depletion reached 42%, 60%, and 72%, below 250, 350, and 450 km, respectively, and the vertically integrated (150–450 km) decrease was 54%. We validated the accuracy of the electron density depletion at 200 km above the Millstone Hill observatory with the incoherent scatter radar observation and at 400 km using the in situ measurement by the Swarm satellite. The coincidence suggests that 3-D tomography is useful for investigating the vertical structure of eclipse-induced ionospheric changes. We further detected the electron depletion and enhancement with maximum values of 1.4–1.9 TECU and 0.7–1.0 TECU, respectively, in the geomagnetic conjugate region in the southern hemisphere.

Plain Language Summary The use of tens of GNSS satellites and thousands of ground GNSS receivers provided us with a rare opportunity to observe the ionospheric changes associated with the great solar eclipse in North America in August 2017. A three-dimensional tomography technique based on total electron content data was used to explore the three-dimensional structure of the ionospheric electron depletion induced by this solar eclipse. We found that a significant electron decrease occurred at a height of ~200 km and the decrease in the *F* region reached ~50%. We also detected simultaneous ionospheric responses to the solar eclipse in the geomagnetic conjugate region in the southern hemisphere.

1. Introduction

During a solar eclipse, the ionospheric electron density decreases rapidly due to the blocking of solar radiation by the Moon. This has been observed by various sensors including ground-based ionosondes (Evans, 1965; Jakowski et al., 2008), incoherent scatter radars (ISRs; Baron & Hunsucker, 1973; MacPherson et al., 2000), and in situ observations from low Earth orbit satellites (Tomás et al., 2007; Wang et al., 2010). Recently, Global Navigation Satellite Systems (GNSS), including the Global Positioning System (GPS), has provided a complementary way to study the ionospheric variations through the total electron content (TEC) changes during solar eclipses (Cherniak & Zakharenkova, 2018; Coster et al., 2017; Ding et al., 2010; Hoque et al., 2016; Le et al., 2008). These past observations have revealed ionospheric responses to solar eclipses characterized by maximum electron density depletions of 10–60% appearing 5–20 min after the totality. Although several papers report observations of vertical structures of ionospheric changes during eclipses using small numbers of ground observatories (Mrak et al., 2018; Stankov et al., 2017), the three-dimensional (3-D) structures of the ionospheric changes over an extensive region have not been obtained.

A total solar eclipse on 21 August 2017 passed over the central part of the continental United States from Oregon to South Carolina. The dense ground GNSS network with continuously operating receivers surrounding the totality path offers a rare opportunity to study the ionospheric response to this event (Figure 1a). Here we present the first tomographic picture of the 3-D structure of the ionospheric electron depletion caused by this eclipse.

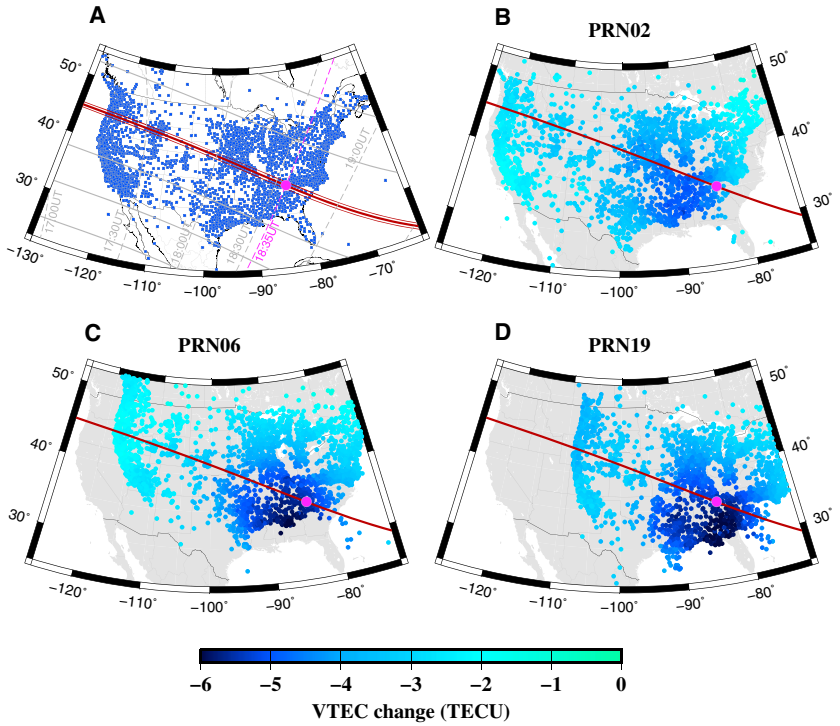

Figure 1. (a) Locations of dense Global Navigation Satellite Systems (GNSS) stations in the continental United States. The thick red solid curve shows the path of the totality. The thin red solid curves show the paths with an eclipse magnitude of 100%, and the gray solid curves show the paths where the eclipse magnitude decreases at a rate of 20%. The blue squares indicate the locations of the GNSS stations used in this study. The dotted gray curves represent the contours of the universal time (UT) of the maximum eclipse with an interval of 30 min, and the dotted magenta curve shows the contour at 18:35 UT. (b–d) The spatial distribution of electron depletion observed with GPS satellites PRN02, 06, and 19. The magenta point shows the region of maximum obscuration at 18:35 UT.

2. Methodology and Data Set

Slant TEC (STEC) is the ionospheric electron density integrated along the line-of-sight (LOS) connecting a GNSS satellite and a ground receiver. This quantity is derived by comparing the time delays of two *L* band signals and expressed in units of 10^{16} el/m^2 (TECU). We first remove the satellite and receiver interfrequency biases following He and Heki (2016). Then we convert these absolute STEC to absolute vertical TEC (VTEC) by multiplying with the cosine of the incident angle of the LOS into a thin shell at 300 km above the ground. To isolate the ionospheric change associated with the solar eclipse, we first calculate the average VTEC of the 3 days, 25, 29, and 30 August 2017, with solar activity similar to that on the eclipse day and under a quiet geomagnetic environment. These days are the only candidates within 1 month (±15 days relative to the eclipse day) that fulfill the selection criteria, that is, $80 < F_{10.7} < 90$, $Dst > -30$ and $Kp < 4+$ (Table S1 in the supporting information). We consider the ~4-min sidereal day shift (Agnew & Larson, 2007) with respect to the eclipse day in combining the VTEC on the three reference days. We then take their average VTEC as the reference curve after adding a constant to let the reference curve match the pre-eclipse part of the eclipse day curve. We define negative departures from the reference curves as the VTEC decrease. We convert all the VTEC residuals back to the LOS directions (the same direction as STEC) and used them as the input to the 3-D reconstruction. Hereafter, we call them slant differential TEC (SDTEC).

To reveal the spatial distribution of the electron depletions caused by the solar eclipse, we conduct 3-D tomography from the SDTEC data using the technique given in He and Heki (2018) and Muafiry et al. (2018). The SDTEC along the *i*th raypath ($SDTEC_i$) can be approximated as the sum of the products of electron density changes and the penetration lengths of voxels. A voxel is an element of a 3-D grid that is bounded in longitude, latitude, and altitude, and the electron density change within one voxel is assumed to be homogeneous. Mathematically,

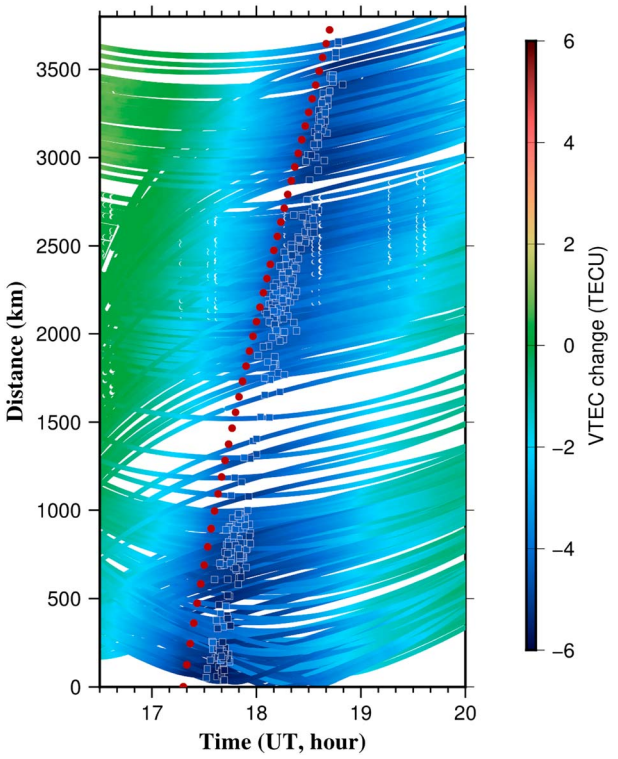

Figure 2. The distance-time diagram of ionospheric depletion for Global Positioning System satellites 2 and 12 during the solar eclipse on 21 August 2017. We only used the ground stations within 1 degree from the totality path. Distances are measured from a point in Oregon (−123.2E, 44.8 N), the start point of the total solar eclipse in United States. The colored squares show the maximum vertical total electron content depletions for individual curve. The velocity of the electron depletion region ranged from 1,080 m/s (over Oregon) to 750 m/s (over South Carolina). The red dotted line shows the location of the eclipse totality.

$$\mathrm{SDTEC}_i = \sum_{j=1}^{n} a_{ij} x_j + \varepsilon_i, \quad (1)$$

where n is the total number of voxels, x_j is the electron density change of the jth voxel, a_{ij} is the length of the ith raypath within the jth voxel, and ε_i is the observation and approximation error for the ith raypath. If the total number of SDTEC measurements is m, equation (1) forms a large sparse system of linear equations **SDTEC** = **AX** + **ε**, where **SDTEC** and **ε** are the measurement and error vectors of m elements, respectively. **A** is the observation coefficient matrix with $m \times n$ components, and **X** is the electron density changes of the n voxels to be estimated. Typically, GNSS ionospheric tomography is an ill-posed problem because m is much less than n. We add a continuity constraint, that is, the electron density changes of adjacent voxels are constrained to have the same value with a reasonable allowance, to regularize the linear least square inversion following (He & Heki, 2018). We set the allowance as 0.05×10^{11} el/m^3 in this study, and the SDTEC observation errors are assumed to be 0.05 TECU, which is a typical error for differential GNSS TEC measurements (Coster et al., 2013).

We used the raw RINEX data from more than 3,600 GNSS stations in North America (Figure 1a). These data are provided by the Continuously Operating Reference Stations of the National Geodetic Survey, the Scripps Orbit and Permanent Array Center, the University NAVSTAR Consortium, the SmartNet North America, and the International GNSS Service. We defined the size of each tomography voxel as 1.5 degrees in longitude, 1.2 degrees in latitude, and 100 km in altitude, ranging from −127°E to −67°E in longitude, 24°N to 54°N in latitude, and 100 km to 1,000 km in altitude. We used SDTEC data between 15 and 23 UT from five GPS satellites, that is, PRN02, 06, 12, 17, and 19, to estimate the 3-D structure of the eclipse-induced ionospheric electron depletion. We employed the elevation mask of 20° for the SDTEC data in this study (Seemala et al., 2014).

3. Results

Figures 1b–1d show the two-dimensional spatial distributions of the VTEC decrease at 18:35 UT (10 min after the greatest eclipse) observed using GPS satellites PRN02 (Figure 1b), 06 (Figure 1c), and 19 (Figure 1d). The dots represent the subionospheric point positions calculated assuming an ionospheric height of 300 km. The electron depletions occurred over the entire continental United States. The different observation angles of the three satellites result in different VTEC decreases; for example, the satellite with a relatively high elevation angle (PRN02) shows a smaller decrease than the one with a lower elevation angle (PRN19), and such varieties facilitate the 3-D tomography. The locations of the largest VTEC drop were similar, extending southward from the totality path, and they reached 5–6 TECU near the shadow zone, that is, 40–50% of the background VTEC. The electron-depleted region moved southeastward with a variable speed of 750–1,080 m/s (Figure 2), and this is consistent with the velocity of the totality.

Figure 3 presents the 3-D distribution of the ionospheric electron density depletion derived from the tomographic reconstruction for eight selected layers with altitudes of 100–800 km at 18:35 UT. Clear ionospheric electron depletions were observed at all the heights. The electron density drops at heights of 100–500 km were much larger than those occurring in the higher altitudes, and the largest drop occurred at the height of 200 km. The depletion observed above 500 km is mainly distributed along the totality path with a relatively small magnitude. For each layer, the centers of maximum depletion at 100–500 km shift southwestward relative to the region of maximum obscuration (magenta point), whereas the depletion area coincides with the totality at higher layers (600–800 km). In general, the changes in the electron density were not synchronous at different heights. We found less depletion in the NE United States at 700–800 km because the maximum reduction of EUV radiation occurred in the SE United States at that time. The obscuration was also less in the NE United States due to the eclipse geometry (Stankov et al., 2017). The smaller background TEC at higher latitudes would also have reduced the electron density drop.

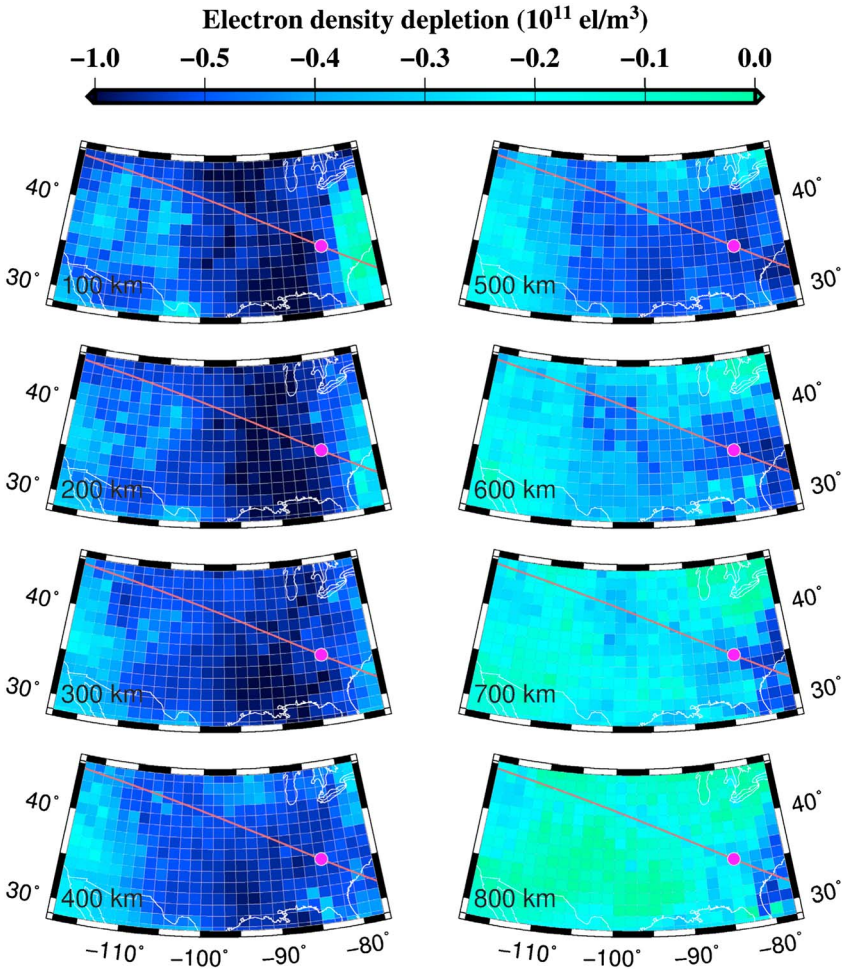

Figure 3. Ionospheric electron density depletion at altitudes from 100 to 800 km derived from 3-D tomography at 18:35 UT. The magenta curve and circle show the totality path trajectory and the region of maximum obscuration at 18:35 UT, respectively. The white curves represent the coastlines and nation boundaries.

4. Discussion and Conclusion

4.1. Accuracy Validation

Before discussing the 3-D structure of electron depletion, we first perform a cross validation to demonstrate the robustness of the tomography. We randomly divide the observation data into two subsets; that is, 90% of data are used for 3-D tomography and 10% are used for validation. We did 3-D tomography using the SDTEC values of only the larger subset. We then compare the calculated and observed VTEC for the smaller subset (Figure 4a) and obtain a root-mean-square difference of 0.48 TECU. This is one order of magnitude smaller than the typical VTEC drops (Figure 1).

It would be meaningful to further validate the tomography results using independent sensors. The Swarm mission, operated by the European Space Agency, provides in situ electron density measurements and offers us an opportunity to validate our results. The Swarm A and C satellites flying side by side with a distance of ~160 km in longitude passed over the continental United States from 18:35 to 18:42 UT at altitudes of 432–438 km. To derive the electron density changes, we used the data from the same satellite on 16 August 2017 (5 days before the eclipse) as a reference. We checked all available Swarm observations in August from 2014 to 2017 and found that, on 16 August 2017, the satellite flew along the trajectory closest in time and space with that on the eclipse day (Figure 4c). We noted that the geomagnetic activity was quiet on 16 August 2017 (Table S1). The Swarm A satellite, at a longitude of ~101°W, observed electron density decreases from 12°N to 67°N in latitude (Figure 4b). We calculated the absolute and relative decreases in electron density by

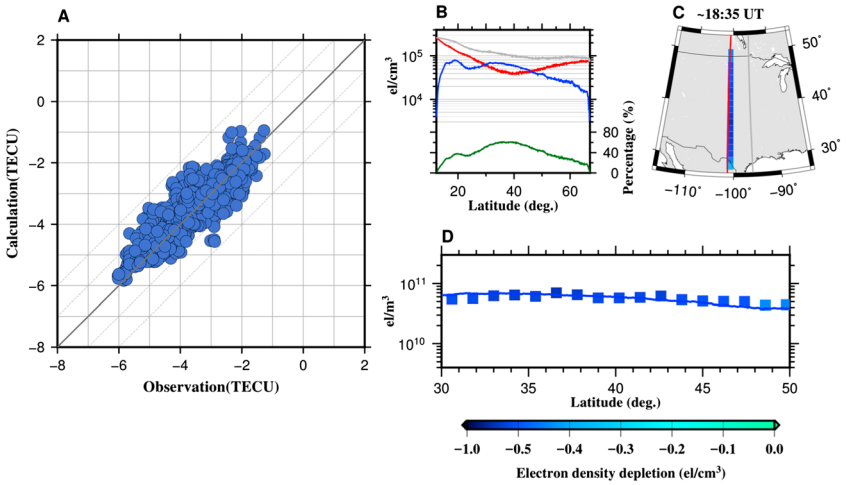

Figure 4. (a) Cross validation of the observed vertical total electron content depletions (10% of the entire data set) at 18:35 UT (horizontal axis) with those calculated from the 3-D tomography results obtained without using these data (vertical axis). (b–d) Comparison of the in situ measurements from the Swarm A satellite with the electron density depletion calculated by 3-D tomography. (b) The in situ electron density observed by Swarm A satellite before the eclipse on 16 August 2017 (gray curve) and during the eclipse on 21 August 2017 (red curve). The blue and green curves show the absolute and relative decreases, respectively. (c) The gray and red curves show the trajectories of Swarm A satellite on 16 August 2017 (the reference day) and on 21 August 2017 (the eclipse day), respectively. The blue squares denote the tomography results within United States at 400 km using the bottom color bar. (d) Comparison between the Swarm observations (blue curve), identical to the blue curve in (b), and the tomography results (blue squares) identical to the blue squares in (c).

comparing the Swarm observations on 21 and 16 August 2017. The maximum absolute decrease was recorded at 30–40°N (blue curve in Figure 4b), and the largest relative decrease was recorded at ~40°N (green curve in Figure 4b), which is close to the intersection with the totality path.

We then compared the Swarm observations with those estimated from our 3-D tomography at an altitude of 400 km, a longitude of 101°W, and latitudes of 30–50°N (Figure 4d). The estimated electron density depletion agreed well with the in situ measurements (Figure 4d). Overall, the comparison between independent measurements demonstrates the reliability of the tomography results associated with the 2017 solar eclipse presented here.

4.2. 3-D Structure of Ionospheric Depletion by the Solar Eclipse

We first stacked the ionospheric electron density changes in all the layers derived from the 3-D reconstruction and made a two-dimensional VTEC anomaly map (Figure 5a). The distribution of the ionospheric depletion coincided well with the result of Coster et al. (2017), although the amplitude of the maximum VTEC decrease showed some difference, that is, −8 TECU in Coster et al. (2017) and −6 TECU in our study. This may be caused by the definition of reference curves; that is, they used the direct VTEC observation as a reference background while we gave a bias to let the two (reference day and eclipse day) curves coincide before the start of the eclipse.

To study the vertical distribution of the ionospheric electron depletion, we made four vertical cross sections from the 3-D tomography results. The profiles along the totality path A-a (Figure 5b) and the longitudinal profile D-d (Figure 5f) cross the region of maximum obscuration at 18:35 UT. We drew two more longitudinal profiles, that is, B-b (Figure 5d) and C-c (Figure 5e). Along the totality path, the decrease in electron density can be found at altitudes up to 800–1,000 km (Figure 5b). In Figures 5d–5f, we found that depletion at high altitudes appears only around the intersection points (red triangles and magenta circle) of profiles and totality path. This suggests that the electron density in the topside ionosphere/plasmasphere slightly decreases only along the path of totality.

We found that the depletion of electron density becomes significant at low altitudes. We take the ionospheric changes below a certain height and divide them by the electron density depletions at all heights to calculate the contributions of different layers. Figure 5c compares the contributions from different heights 150–850 km

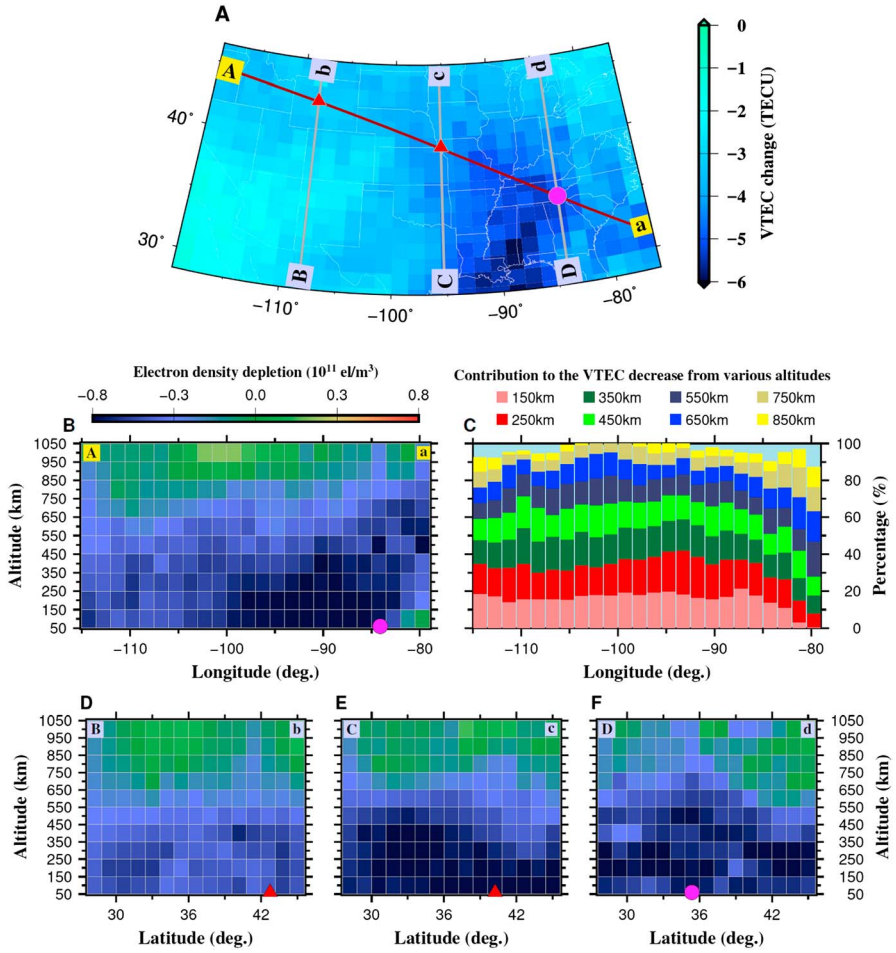

Figure 5. Vertical cross sections of the ionospheric electron depletion associated with the 21 August 2017 solar eclipse. (a) Map of the vertically integrated electron depletion from the 3-D tomography results. We also show the locations of the three longitudinal cross sections given in (d)–(f) with gray lines. The red curve represents the totality path of the solar eclipse. The white lines show the coast and state borders of the United States. The magenta circle shows the region of maximum obscuration at 18:35 UT. The red triangles show the intersection points of profiles and the totality path, which again appear in (d)–(f). (b) Section of the 3-D tomography results of electron density anomalies along the totality path. (c) The contributions to the vertical total electron content changes from parts with various altitudes (150–850 km with a step of 100 km). (d–f) Sections from 3-D tomography results at −118, −106, and −94 degrees in longitude. We used the same color bar as in (b).

with an interval of 100 km. We found that the maximum relative decrease (up to 25%) occurred at the height range 150–250 km. The relative decreases below 250, 350, and 450 km are ~42%, ~60%, and ~72%, respectively, and the integrated decrease from 150 to 450 km was 54%. We also note that the largest decrease occurred at higher altitudes above the southeastern corner of United States. However, this may simply reflect errors in constraining the electron depletion due to the insufficient numbers of raypaths at the edge of the studied region.

These results can be compared with various observations and numerical simulations. For example, Huba and Drob (2017) used the SAMI3 simulation to predict that the electron density may decrease down to ~50% in the *F* region during this solar eclipse. Le et al. (2008, 2010) used ionosonde and GNSS occultation to clarify the vertical profile of the midlatitude ionospheric response and found the largest electron density decrease at ~200 km. Recently, Goncharenko et al. (2018) reported the electron density changes caused by this eclipse at Millstone Hill (~1,000 km away from the totality zone) observed using ISR. The largest decrease occurred at height 200–300 km, and this is consistent with our results. According to our 3-D tomography, the electron density decrease at 18:35 UT, 200 km above the Millstone Hill observatory (42.6N, −71.5E), was

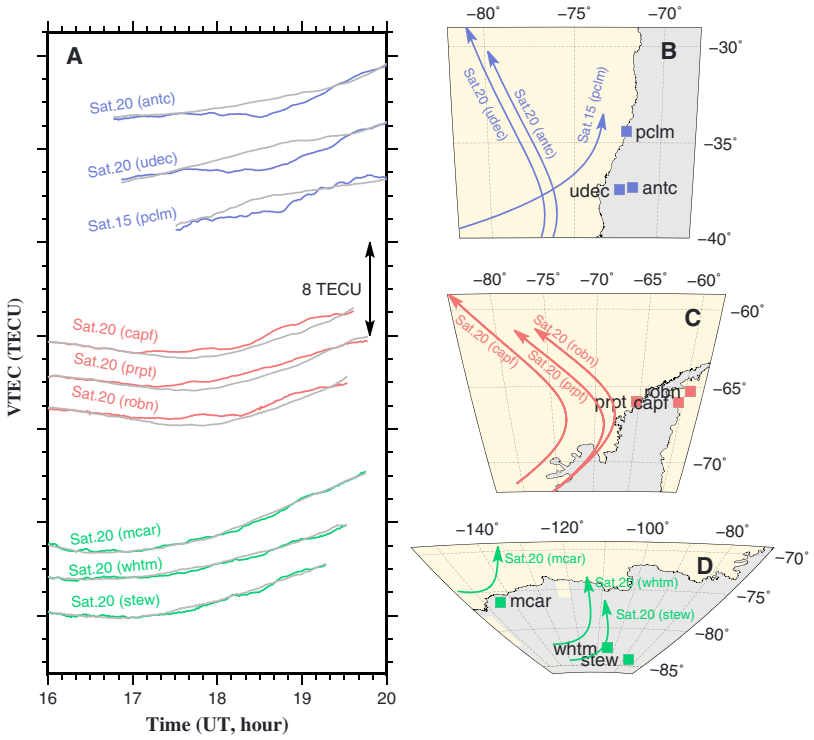

Figure 6. Possible ionospheric total electron content (TEC) decrease and enhancement observed in the geomagnetic conjugate region in the southern hemisphere during the 21 August 2017 solar eclipse. (a) Vertical TEC (VTEC) time series observed with three pairs of station-satellite showing electron decreases (upper blue curves) and increases (middle red curves), respectively. We also show VTEC time series without anomalies (lower green curves) observed at three Global Navigation Satellite Systems (GNSS) stations far from the conjugate region influenced by the eclipse. We used the same procedure to derive the reference curves (gray curves) as in North America. (b–d) The maps showing the locations of GNSS stations (colored squares) and the subionospheric point (SIP) trajectories (colored curves). GNSS satellite (they are all GPS) numbers and GNSS station names are attached to the curves. We assumed 300 km for ionospheric height in drawing SIP tracks.

0.65×10^{11} el/m^3, which is only slightly smaller than the ISR observational result (~0.75×10^{11} el/m^3). This small difference might be due to the relatively high geomagnetic activity on the reference day (22 August 2017) used by Goncharenko et al. (2018).

The changes of electron density in the ionosphere at different heights during solar eclipses depend on different physical processes such as photochemistry below the F2 layer and transport at the F2 layer and higher altitudes (Jakowski et al., 2008; Le, Liu, Yue, Wan, & Ning, 2009). The large electron depletion and nonuniform latitudinal response (relative to the totality path) in the lower ionosphere for this eclipse may reflect the two factors: (i) Ion recombination was more effective at lower altitudes because of the larger neutral molecule density, and (ii) the decrease of ion temperature caused the reduction in plasma pressure and promoted downward flux along the magnetic field (Le et al., 2010). In addition, it is important to mention that the eclipse geometry and the latitude dependence of the background TEC are of crucial significance to form the reconstructed 3-D structure of electron density depletion.

4.3. Electron Increase and Depletion in the Geomagnetic Conjugate Region

The ionosphere in the conjugated region may respond synchronously to solar eclipses (Huba & Drob, 2017; Le, Liu, Yue, & Wan, 2009). During the 2017 event, the decrease in conductivity over a continent-size region leads to the enhancement of electrostatic potential over the United States. This also increases the electrostatic potential in the geomagnetic conjugate region in the opposite hemisphere. The SAMI3 simulation predicts a gentle enhancement of TEC, smaller than 1 TECU, in the conjugate region near the Antarctic Peninsula (Huba & Drob, 2017). It also predicts a delayed electron depletion to the west of South America, primarily due to the electron redistribution by the $\boldsymbol{E} \times \boldsymbol{B}$ drift. We found several GNSS stations located in these two regions

(Figures 6b and 6c). We derived the reference curve using the same procedure as in North America (average of VTEC on 3 days, 25, 29, and 30 August 2017). We observed VTEC decreases (blue curves in Figure 6a) and enhancements (red curves in Figure 6a) with GPS satellites 15 and 20, respectively, in the expected region (Figures 6b and 6c). The largest VTEC decreases and increases are 1.4–1.9 TECU and 0.7–1.0 TECU, respectively.

To show that significant VTEC changes occurred only in the prescribed region, we show three VTEC time series without anomalies (green curves in Figure 6a) observed at stations far from the conjugate region influenced by this eclipse estimated by Huba and Drob (2017). The positions of these GNSS sites and subionospheric point trajectories are shown in Figure 6d. They show insignificant departures from the reference curves and suggest that eclipse-induced signatures are negligible in the far field. We note that the amplitude of the observed conjugate TEC change is slightly larger than the predicted value (the observed TEC decrease was also stronger than predicted over the continental United States). Here we confirmed that the locations of the observed ionospheric depletions and enhancements are consistent with the SAMI3 prediction, but this still needs to be substantiated with observations by other sensors.

Acknowledgments
We thank two reviewers for constructive comments. Liming He was supported by the National Natural Science Foundation of China (grant 41104104) and by the Key Laboratory of Geospace Environment and Geodesy, Ministry of Education, Wuhan University (grant 17-01-03). We downloaded GNSS data from National Geodetic Survey (http://www.ngs.noaa.gov), Scripps Orbit and Permanent Array Center (http://sopac.ucsd.edu), University NAVSTAR Consortium (http://www.unavco.org), SmartNet North America (https://www.smartnetna.com), and International GNSS Service (http://www.igs.org). We thank European Space Agency for providing the Swarm data (https://earth.esa.int/swarm).

References

Agnew, D. C., & Larson, K. M. (2007). Finding the repeat times of the GPS constellation. *GPS Solutions*, *11*(1), 71–76.
Baron, M., & Hunsucker, R. (1973). Incoherent scatter radar observations of the auroral zone ionosphere during the total solar eclipse of July 10, 1972. *Journal of Geophysical Research*, *78*(31), 7451–7460. https://doi.org/10.1029/JA078i031p07451
Cherniak, I., & Zakharenkova, I. (2018). Ionospheric total electron content response to the great American solar eclipse of 21 August 2017. *Geophysical Research Letters*, *45*, 1199–1208. https://doi.org/10.1002/2017GL075989
Coster, A., Williams, J., Weatherwax, A., Rideout, W., & Herne, D. (2013). Accuracy of GPS total electron content: GPS receiver bias temperature dependence. *Radio Science*, *48*, 190–196. https://doi.org/10.1002/rds.20011
Coster, A. J., Goncharenko, L., Zhang, S.-R., Erickson, P. J., Rideout, W., & Vierinen, J. (2017). GNSS observations of Ionospheric variations during the 21 August 2017 solar eclipse. *Geophysical Research Letters*, *44*, 12,041–12,048. https://doi.org/10.1002/2017GL075774
Ding, F., Wan, W., Ning, B., Liu, L., Le, H., Xu, G., et al. (2010). GPS TEC response to the 22 July 2009 total solar eclipse in East Asia. *Journal of Geophysical Research*, *115*, A07308. https://doi.org/10.1029/2009JA015113
Evans, J. V. (1965). On the behavior of *f*0F2 during solar eclipses. *Journal of Geophysical Research*, *70*(3), 733–738. https://doi.org/10.1029/JZ070i003p00733
Goncharenko, L. P., Erickson, P. J., Zhang, S.-R., Galkin, I., Coster, A. J., & Jonah, O. F. (2018). Ionospheric response to the solar eclipse of 21 August 2017 in Millstone Hill (42N) observations. *Geophysical Research Letters*, *45*, 4601–4609. https://doi.org/10.1029/2018GL077334
He, L., & Heki, K. (2016). Three-dimensional distribution of ionospheric anomalies prior to three large earthquakes in Chile. *Geophysical Research Letters*, *43*, 7287–7293. https://doi.org/10.1002/2016GL069863
He, L., & Heki, K. (2018). Three-dimensional tomography of ionospheric anomalies immediately before the 2015 Illapel earthquake, Central Chile. *Journal of Geophysical Research: Space Physics*, *123*, 4015–4025. https://doi.org/10.1029/2017JA024871
Hoque, M. M., Wenzel, D., Jakowski, N., Gerzen, T., Berdermann, J., Wilken, V., et al. (2016). Ionospheric response over Europe during the solar eclipse of March 20, 2015. *Journal of Space Weather and Space Climate*, *6*, A36. https://doi.org/10.1051/swsc/2016032
Huba, J. D., & Drob, D. (2017). SAMI3 prediction of the impact of the 21 August 2017 total solar eclipse on the ionosphere/plasmasphere system. *Geophysical Research Letters*, *44*, 5928–5935. https://doi.org/10.1002/2017GL073549
Jakowski, N., Stankov, S. M., Wilken, V., Borries, C., Altadill, D., Chum, J., et al. (2008). Ionospheric behavior over Europe during the solar eclipse of 3 October 2005. *Journal of Atmospheric and Solar - Terrestrial Physics*, *70*(6), 836–853. https://doi.org/10.1016/j.jastp.2007.02.016
Le, H., Liu, L., Yue, X., & Wan, W. (2008). The ionospheric responses to the 11 August 1999 solar eclipse: Observations and modeling. *Annales de Geophysique*, *26*(1), 107–116. https://doi.org/10.5194/angeo-26-107-2008
Le, H., Liu, L., Yue, X., & Wan, W. (2009). The ionospheric behavior in conjugate hemispheres during the 3 October 2005 solar eclipse. *Annales de Geophysique*, *27*(1), 179–184. https://doi.org/10.5194/angeo-27-179-2009
Le, H., Liu, L., Yue, X., Wan, W., & Ning, B. (2009). Latitudinal dependence of the ionospheric response to solar eclipses. *Journal of Geophysical Research*, *114*, A07308. https://doi.org/10.1029/2009JA014072
Le, H., Liu, L., Ding, F., Ren, Z., Chen, Y., Wan, W., et al. (2010). Observations and modeling of the ionospheric behaviors over the East Asia zone during the 22 July 2009 solar eclipse. *Journal of Geophysical Research*, *115*, A10313. https://doi.org/10.1029/2010JA015609
MacPherson, B., Gonzalez, S., Sulzer, M., Bailey, G., Djuth, F., & Rodriguez, P. (2000). Measurements of the topside ionosphere over Arecibo during the total solar eclipse of February 26, 1998. *Journal of Geophysical Research*, *105*(A10), 23,055–23,067. https://doi.org/10.1029/2000JA000145
Mrak, S., Semeter, J. L., Drob, D., & Huba, J. D. (2018). Direct EUV/X-ray modulation of the ionosphere during the August 2017 total solar eclipse. *Geophysical Research Letters*, *45*, 3820–3828. https://doi.org/10.1029/2017GL076771
Muafiry, I. N., Heki, K., & Maeda, J. (2018). 3D tomography of midlatitude sporadic-E in Japan from GNSS-TEC data. *Earth, Planets and Space*, *70*(1), 45. https://doi.org/10.1186/s40623-018-0815-7
Seemala, G. K., Yamamoto, M., Saito, A., & Chen, C.-H. (2014). Three-dimensional GPS ionospheric tomography over Japan using constrained least squares. *Journal of Geophysical Research: Space Physics*, *119*, 3044–3052. https://doi.org/10.1002/2013JA019582
Stankov, S. M., Bergeot, N., Berghmans, D., Bolsée, D., Bruyninx, C., Chevalier, J. M., et al. (2017). Multi-instrument observations of the solar eclipse on 20 March 2015 and its effects on the ionosphere over Belgium and Europe. *Journal of Space Weather and Space Climate*, *7*, A19. https://doi.org/10.1051/swsc/2017017
Tomás, A. T., Lühr, H., Förster, M., Rentz, S., & Rother, M. (2007). Observations of the low-latitude solar eclipse on 8 April 2005 by CHAMP. *Journal of Geophysical Research*, *112*, A06303. https://doi.org/10.1029/2006JA012168
Wang, X., Berthelier, J. J., & Lebreton, J. P. (2010). Ionosphere variations at 700 km altitude observed by the DEMETER satellite during the 29 March 2006 solar eclipse. *Journal of Geophysical Research*, *115*, A11312. https://doi.org/10.1029/2010JA015497